2025 13th International Conference on Intelligent Computing and Wireless Optical Communications (ICWOC) | 979-8-3315-4480-5/25/$31.00 ©2025 IEEE | DOI: 10.1109/ICWOC65853.2025.11150801

Intelligent Modulation Recognition for Generalized Optical MIMO in OWC Systems

1st Xinyue Zhang
School of Microelectronics and Communication Engineering
Chongqing University
Chongqing 400044, China
202212021043t@stu.cqu.edu.cn

2nd Zhihong Zeng
School of Microelectronics and Communication Engineering
Chongqing University
Chongqing 400044, China
zhihong.zeng@cqu.edu.cn

3rd Dengke Wang
School of Microelectronics and Communication Engineering
Chongqing University
Chongqing 400044, China
dengke.wang@cqu.edu.cn

4th Chen Chen*
School of Microelectronics and Communication Engineering
Chongqing University
Chongqing 400044, China
c.chen@cqu.edu.cn
*Corresponding author

***Abstract*—A modulation recognition method for generalized optical multiple-input multiple-output (GO-MIMO) schemes in optical wireless communication (OWC) systems is proposed, which employs the frequency domain difference amplitude histogram as a feature to complete the identification of the two schemes. The proposed method has a low-complexity advantage and achieves highly accurate recognition at low signal-to-noise ratios (SNRs).**

***Index Terms*—Optical wireless communication, automatic modulation recognition, generalized optical MIMO**

I. Introduction

Optical wireless communication (OWC) has emerged as a key enabling technology for 6G networks, offering substantial advantages including abundant spectrum resources, ultra-low latency, enhanced security, high capacity, and cost-effectiveness [1]. In OWC systems, light-emitting diodes (LEDs) and photodetectors (PDs) are used as transmitter and receiver units, respectively. However, these components tend to have low-pass characteristics, resulting in a limited system bandwidth [2]. To break through this limitation, multiple-input multiple-output (MIMO) technique is introduced into OWC systems. Spatial modulation (SM), as the simplest MIMO digital scheme, selects only one transmitter to transmit the signal at each time instant [3]. To further enhance conventional SM, generalized spatial modulation (GSM) has been introduced in OWC systems, activating multiple antennas to transmit the same information, thereby improving transmission performance [4]. The combination of MIMO with orthogonal frequency division multiplexing (OFDM) modulation technique can significantly enhance the capacity of band-limited OWC systems. Lately, the combination of GSM and OFDM in MIMO transmission has been widely used in band-limited OWC systems. To distinguish between two different types of GSM schemes, the scheme that transmits the same signal with activated transmitters as GSM, and the scheme that transmits different signals with activated transmitters as GSMP [5]. Specifically, the transmission scenarios that combine OFDM and are mapped in the frequency domain are defined as FD-GSM and FD-GSMP, respectively.

To perform demodulation in generalized optical MIMO (GO-MIMO) systems, the transmission schemes and the exact number of activated LEDs need to be known at the receiver side. Considering the practical OWC channel can be complex and dynamic, in OFDM-based GO-MIMO systems, adaptive modulation schemes can be implemented depending on the channel conditions. Hence, it is of practical significance to enable modulation recognition at the receiver side before carrying out signal demodulation. Currently, research on modulation recognition in OWC has been reported [6], [7], [8]. In [7], the index recognition for OFDM-IM was accomplished using frequency domain histograms, while [8] accomplished the recognition of specific index schemes and modulation formats. However, research on GSM-related modulation recognition remains limited. Study by [9] demonstrated the superior classification accuracy of QAM over FSK in SM, QSM, and GSM scenarios, while revealing notably high misclassification rates for QSM and conventional SM. Moreover, [10] achieved 95% recognition accuracy at 130 dB in 2×2 MIMO systems using an SNN-based approach with just four sampling points, but with substantial computational complexity.

In this paper, we propose an intelligent modulation recognition scheme for OFDM-based FD-GSM and FD-GSMP in GO-MIMO systems by exploiting frequency domain difference amplitude histograms as the recognition features. Moreover, machine learning and deep learning algorithms including decision trees (DT), support vector machine (SVM), k-nearest

neighbors (k-NN) and convolutional neural network (CNN) are applied to perform intelligent modulation recognition based on the histograms. Simulations are conducted to verify the feasibility of the proposed intelligent modulation recognition scheme for OFDM-based FD-GSM and FD-GSMP in GO-MIMO systems.

II. System Model

In this section, we first introduce the channel model of a typical OWC-MIMO system and then introduce the basic assumptions of the modulation recognition task along with the recognition objectives.

A. Channel Model of a Typical OWC-MIMO System

In a typical model of a GO-MIMO system based on IM/DD technology, the signals are sent by N_t transmitters (LEDs) and simultaneously received by N_r receivers (PDs). Consider the transmitted signal vector is defined as $\mathbf{x} = [x_1, x_2, \ldots, x_{N_t}]^{\mathrm{T}}$ and $\mathbf{H}$ denote the $N_r \times N_t$ channel matrix, then the received signal vector $\mathbf{y} = [y_1, y_2, \ldots, y_{N_r}]^{\mathrm{T}}$ after transmission through the OWC channel can be expressed as

$$\mathbf{y} = \mathbf{H}\mathbf{x} + \mathbf{n}, \tag{1}$$

where $\mathbf{n} = [n_1, n_2, \ldots, n_{N_r}]^{\mathrm{T}}$ presents the additive noise vector, and the channel matrix $\mathbf{H}$ can be further expressed as:

$$\mathbf{H} = \begin{bmatrix} h_{11} & h_{12} & \cdots & h_{1N_t} \\ h_{21} & h_{22} & \cdots & h_{2N_t} \\ \vdots & \vdots & \ddots & \vdots \\ h_{N_r1} & h_{N_r2} & \cdots & h_{N_rN_t} \end{bmatrix}. \tag{2}$$

In (2), each element h_{rt} represents the direct current (DC) channel gain between the t-th LED and the r-th PD. The channel DC gain of an indoor OWC system consists of the Line of Sight (LOS) component and the Non-Line of Sight (NLOS) component, which are divided according to the different transmission paths of the optical signals. As shown

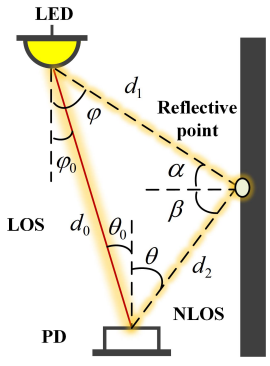

Fig. 1. Diagram of LOS link and NLOS link for indoor-OWC system.

in Fig.1, for the link between the t-th LED and r-th PD, the LOS component of the channel DC gain can be expressed as [11]:

$$h_{rt,\mathrm{LOS}} = \begin{cases} \frac{(m+1)\rho A}{2\pi d_0^2}\cos^m(\varphi_0)T_s(\theta_0)g(\theta_0)\cos(\theta_0), \\ \text{for } 0 \le \theta_0 \le \phi \\ 0, \ \text{for } \theta_0 > \phi \end{cases}, \tag{3}$$

where ρ and A represent responsivity and effective area of the PD, respectively; d_0 denotes the distance between the t-th LED and r-th PD; φ_0 and θ_0 are the irradiation angle of the LED and the incident angle of the PD, respectively; $T_s(\theta_0)$ is the optical filter gain (set to 1 when no filter exists); and $g(\theta_0) = n^2/\sin^2\phi$ represents the gain of optical lens, where n and ϕ denote the refractive index and the half-angle field-of-view (FOV) of the optical lens, respectively.

For the NLOS link, the light emitted from the LED diverges at angle φ, reflects off a surface, and then reaches the PD. Here, α represents the incident angle to the reflective point with distance d_1 from the t-th LED, while the reflected light travels distance d_2 to the r-th PD with angle β which is the angle of irradiance from the reflective point. Thus, the NLOS component of the channel DC gain can be expressed as [12]:

$$h_{rt,\mathrm{NLOS}} = \begin{cases} \int \frac{(m+1)\rho\varepsilon A}{2(\pi d_1 d_2)^2}\cos^m(\varphi)\cos(\alpha)\cos(\beta)\times \\ T_s(\theta)g(\theta)\cos(\theta)dA_\omega, \ \text{for } 0 \le \theta \le \phi \\ 0, \ \text{for } \theta > \phi \end{cases}, \tag{4}$$

where dA_ω is a small reflective area on the wall and ε is the reflectance coefficient of the wall.

B. Modulation Recognition for GO-MIMO

In FD-GSM and FD-GSMP, ML detection is used at the receiver side to estimate the constellation symbol vectors and spatial index vectors to recover the constellation bits and spatial bits. However, the prerequisite for ML detection is that the number of active OFDM modulators at the transmitter side is known, and thus the number of active modulators, i.e., the number of LEDs, needs to be identified in the two schemes mentioned.

Taking a 2×2 MIMO system as an example, i.e., the number of LEDs N_t and the number of PDs N_r are both 2, Table I shows the mapping table of FD-GSM and FD-GSMP. Note that when $N = 1$, both OFDM-based FD-GSM and FD-GSMP activate one LED to send constellation symbols, which is equivalent to the traditional SM, and thus can be regarded as the same scheme. The objective is to accomplish the recognition task of transmission schemes and the number of active LEDs under the following assumptions:

Assumption A1: The number of transmitters (LEDs) N_t and receivers (PDs) N_r in the GO-MIMO system are known, constituting a 2×2 MIMO system.

Assumption A2: Over T OFDM symbols, the constellation order M and the number of active OFDM modulators remain unchanged.

Assumption A3: When $N = 1$, FD-GSMP and FD-GSM are equivalent to traditional SM, representing the same scheme. Therefore, a total of 3 schemes need to be identified,

TABLE I
OFDM-BASED FD-GSM AND FD-GSMP MAPPING TABLE FOR $N_t = 2$ AND $N = 1, 2$

Scheme	Active Count	Spatial Bit	LED #1	LED #2
FD-GSM	$N = 1$	0	c	0
		1	0	c
	$N = 2$	/	c	c
FD-GSMP	$N = 1$	0	c	0
		1	0	c
	$N = 2$	/	c_1	c_2

including the transmission scheme and the number of active modulators: FD-GSM with $N = 1$, FD-GSM with $N = 2$, and FD-GSMP with $N = 2$.

Based on these assumptions, we aim to address the recognition of specific transmission schemes and the number of active LEDs in OFDM-based FD-GSM and FD-GSMP systems, providing support for correct demodulation at the receiver.

III. Proposed Modulation Classification Method

In this section, we introduce the extraction of frequency-domain difference amplitude histogram features and present the classification algorithms for identifying both the transmission scheme and the number of activated LEDs.

A. Feature Extraction

The frequency-domain transmitted signal vector for both FD-GSM and FD-GSMP schemes at a given subcarrier slot can be represented as $x_F = [x_{1,F}, x_{2,F}, \ldots, x_{N_t,F}]^T$. For each element $x_{k,F}$ ($k = 1, 2, \ldots, N_t$), inactive LEDs (when k is outside the activation range) have $x_{k,F} = 0$, while active LEDs exhibit different behavior: in FD-GSM, $x_{k,F}$ equals the constellation symbol c, whereas in FD-GSMP, $x_{k,F}$ takes distinct symbols c_i across different OFDM modulators.

For a 2×2 GO-MIMO system, the FD-GSM transmitted signal at a given subcarrier can be defined as $x_{\text{FD-GSM}} = [x_1, x_2]^T$, when $N = 1$, $x_{\text{FD-GSM}} = [c, 0]^T$ or $[0, c]^T$; and when $N = 2$, $x_{\text{FD-GSM}} = [c, c]^T$. Similarly, for FD-GSMP when $N = 2$, the transmitted signal can be expressed as $x_{\text{FD-GSMP}} = [c_1, c_2]^T$, where c_1 and c_2 represent distinct constellation symbols from different OFDM modulators.

For the frequency-domain signal characteristics under both transmission schemes, in FD-GSM, when subtracting the two frequency-domain signals and taking the absolute value at a given subcarrier with $N = 1$:

$$|x_{\text{FD-GSM}}|' = |x_1 - x_2| = |c|; \tag{5}$$

and with $N = 2$:

$$|x_{\text{FD-GSM}}|' = |x_1 - x_2| = |c - c| = 0. \tag{6}$$

Similarly, for FD-GSMP with $N = 2$:

$$|x_{\text{FD-GSMP}}|' = |c_1 - c_2|. \tag{7}$$

Equations (5)-(7) show distinct frequency-domain difference amplitudes: $|c|$ (FD-GSM, $N = 1$), 0 (FD-GSM, $N = 2$), and $|c_1 - c_2|$ (FD-GSMP, $N = 2$). These distinct frequency-domain difference signal magnitudes can serve as distinguishing features among the three schemes.

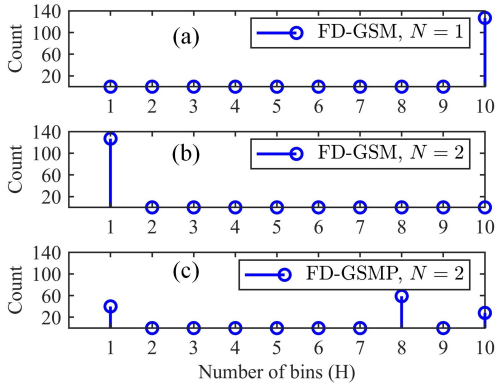

Fig. 2. Transmitted signal histograms without normalization for (a) FD-GSM, $N = 1$, (b) FD-GSM, $N = 2$, and (c) FD-GSMP, $N = 2$.

To eliminate the influence of signal amplitude and better compare the frequency-domain signal differences between different schemes, after subtracting the two signals, normalization is performed. Specifically, using the complex-valued signal vector received in the frequency domain for the t-th OFDM symbol, after subtracting the two signals and taking the absolute value, the signal can be expressed as $|x^t|$, which is then normalized to the [0,1] interval to obtain $\hat{x}_i^t$:

$$\hat{x}_i^t = \frac{|x_i^t| - |x_{\min}^t|}{|x_{\max}^t| - |x_{\min}^t|}, \tag{8}$$

where $x_{\max}^t$ and $x_{\min}^t$ denote the maximum and minimum values of the difference signal, respectively.

The obtained frequency-domain difference amplitudes are divided into H intervals, where the frequency counts reflect the distribution characteristics of differential amplitudes across intervals. Based on this, a histogram feature distribution vector is extracted. Multiple symbols are jointly employed to generate the signal feature histogram to further suppress additive noise interference and enhance the stability and reliability of feature extraction, where the number of symbols is defined as T.

Fig. 2 illustrates the un-normalized histograms of the transmitted signals under the three to-be-recognized schemes in the ideal case (no noise). When $N = 1$, the histogram of OFDM-based FD-GSM concentrates in the last interval with the amplitudes near 1. For $N = 2$ in FD-GSM, all difference amplitudes fall in the first interval (zero values), consistent with (6) where identical symbols from two LEDs produce zero difference. In contrast, FD-GSMP with $N = 2$ shows widely distributed amplitudes. These fundamentally different histogram distributions provide a theoretical basis for distinguishing the three transmission schemes.

B. Classification Algorithms

Fig.3 shows the block diagram of GO-MIMO modulation recognition based on feature extraction. The GO-MIMO symbols to be recognized first undergo signal preprocessing, and

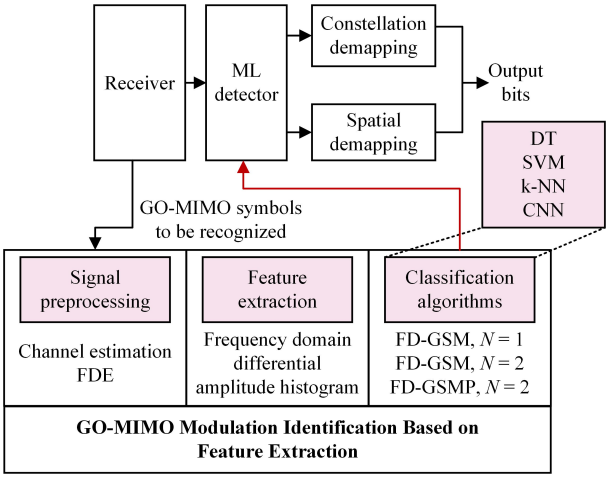

Fig. 3. Block diagram of GO-MIMO modulation recognition based on feature extraction.

then the frequency domain signals are obtained by the FFT transform, and the amplitude histograms of the frequency domain difference signals are obtained by taking the absolute value of the difference between the two frequency domain signals and normalizing them. The extracted histogram feature vectors form a dataset, which is combined with four classification algorithms, including DT, SVM, k-NN, and CNN, for the recognition of the corresponding transmission schemes and the number of actived LEDs.

IV. Results and Discussions

In this section, we demonstrate the proposed modulation recognition method by simulation, firstly introduce the constructed indoor GO-MIMO system, and then analyse the simulation results.

A. Simulation Setup

As shown in Fig.4, the GO-MIMO system is set up in a 4 m × 4 m × 3 m indoor room in the simulation. Specifically, for the 2×2 MIMO system, the LED array is located in the centre of the ceiling at a height of 3 m, and the receiving plane where the PD is located is at a height of 0.85 m from the floor. The distance between the two LEDs is 2 m, and the distance between the two APDs is 0.1 m. To achieve full coverage, the semi-angle of half power of LEDs and the half-angle FOV of optical lens are both set to 65°, and other detailed parameters are shown in Table II. The large transmitted-to-received signal-to-noise ratio (SNR) difference arises from channel path loss in free-space optical analysis. For indoor GO-MIMO systems, typical channel gains (10^{-5} to 10^{-6}) correspond to 100-120 dB path loss, resulting in received SNR being 100-120 dB lower than transmitted SNR.

The histogram samples used for training and testing are generated according to the method described in the previous section, and the modulation format is 4-QAM. As shown in the Table III, 400 sample signals are collected for each transmission scheme for each SNR condition, and a total of

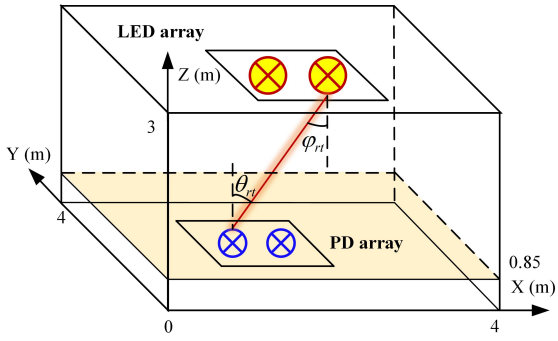

Fig. 4. Geometric setup of a general GO-MIMO system.

TABLE II
Parameter Settings for GO-MIMO System Simulation

Parameter	Value
Room dimension	4 m × 4 m × 3 m
Height of Receiving plane	0.85 m
Semi-angle of half power of LED	65°
Number of LEDs N_t	2
Activated LEDs N	1, 2
LED spacing	2 m
Number of APDs N_r	2
APD spacing	0.1 m
Active area of APD	19.6 mm^2
Responsivity of APD	15 A/W
Gain of optical filter	0.9
Refractive index of optical lens	1.5
Half-angle FOV of optical lens	65°
Reflectance coefficient of wall	0.8
Modulation bandwidth	20 MHz
Noise power spectral density	10^{-22} A^2/Hz

1,200 data samples are generated for the three transmission schemes. Each data sample consists of the feature distribution vector of the histogram with the number of bins (H). The generated dataset is divided into the training set and the test set in the ratio of 4:1, containing 960 and 240 samples, respectively.

TABLE III
Parameters for Signal Generation in Simulation

Parameter	Value
IFFT/FFT size N_{F}	256
Data subcarriers N_{data}	127
Transmission schemes	FD-GSM and FD-GSMP
Number of symbols	1000
Modulation order M	4-QAM
Transmitted SNR	100 dB-123 dB
Received SNR	0 dB-22 dB
Number of sample signals	400 per scheme (1200 total)

B. Simulation Results and Discussions

Fig. 5 shows the normalized feature histograms for the three transmission schemes using 4-QAM at $T = 1$, H = 10. For FD-GSM with $N = 1$, the histogram distribution with normalized amplitudes spanning all intervals, showing a characteristic middle-peaked shape. For FD-GSM with $N = 2$, the histogram distribution is theoretically around zero, practical

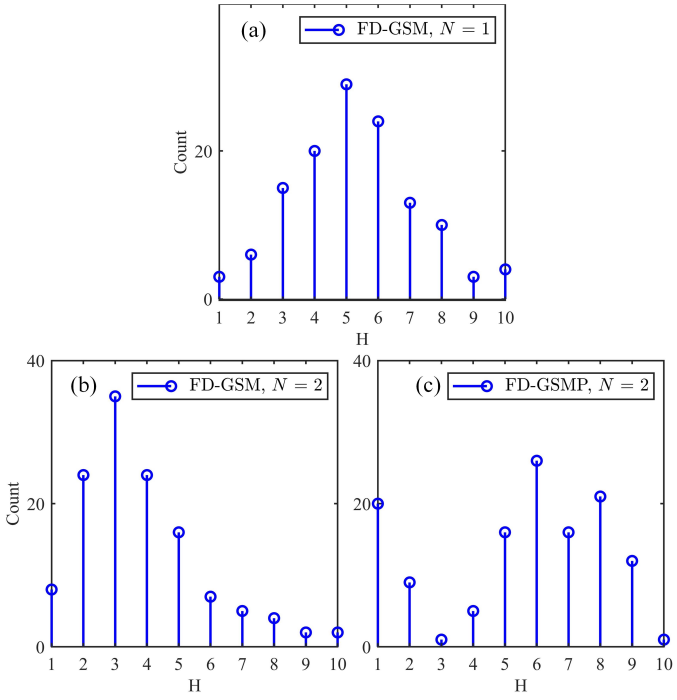

Fig. 5. Received signal histograms with normalization for (a) FD-GSM, $N = 1$, (b) FD-GSM, $N = 2$, and (c) FD-GSMP, $N = 2$.

NLOS effect and channel noise introduce small variations, thus concentrating amplitudes in lower-value intervals. For FD-GSMP with $N = 2$, the histogram distribution shows the difference between the two different signals, different from the FD-GSM cases. Specifically, for FD-GSM, the non-zero differences primarily result from channel gain variations and noise, manifesting as small-amplitude fluctuations centered around zero, which directly reflect the channel conditions and noise level. In contrast, FD-GSMP reflects different information through the two channels, making the information disparity the dominant factor for non-zero differences, thus leading to significant amplitude dispersion with peak values distinctly offset from zero.

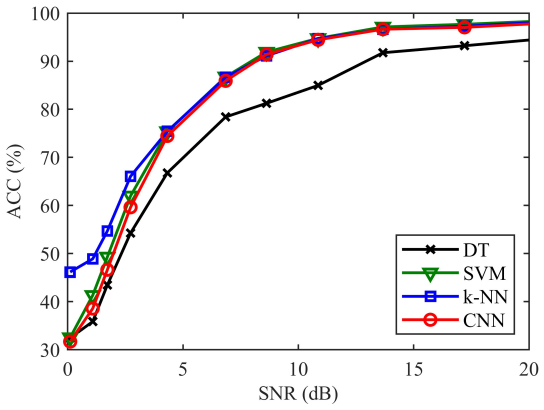

Fig. 6. ACC vs. SNR with four classification algorithms.

Fig. 6 shows the recognition accuracy (ACC) versus received SNR for different algorithms in an OFDM-based GO-MIMO system using 4-QAM, with $T = 1$ and H = 10. The results demonstrate that all classification algorithms exhibit improved ACC with increasing SNR. Moreover, the DT algorithm shows the poorest performance, while the other three algorithms achieve comparable results. Specifically, when using just one OFDM symbol, classification algorithms (excluding DT) require 8.6 dB to exceed 90% ACC, and require 20 dB to reach 98% ACC. These requirements highlight the challenging nature of the classification task in the GO-MIMO system.

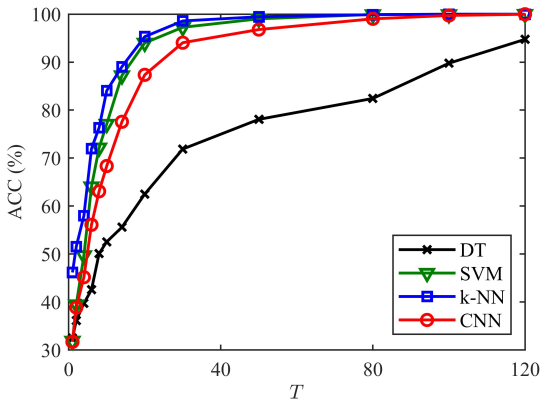

Fig. 7. ACC vs. number of symbols (T).

Fig. 7 shows the recognition accuracy versus number of symbols with different recognition algorithms using 4-QAM, for H = 10 and SNR = 0.1 dB, where the accuracy can be substantially improved by increasing the number of symbols (T) used to generate the feature histograms. Specifically, at 0.1 dB, when T is increased from 1 to 20, the accuracy of k-NN increases from 46.2% to 95.3%, and when 120 symbols are used, the accuracy reaches 100%.

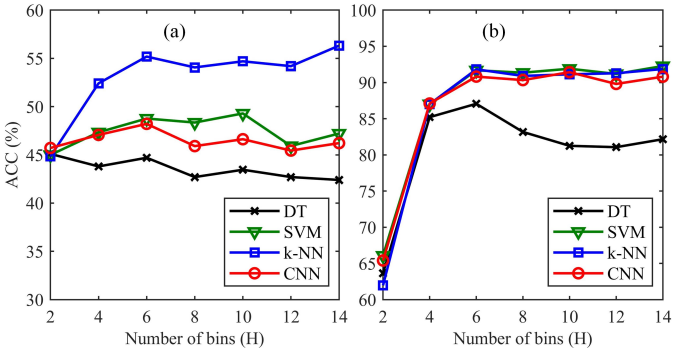

Fig. 8. ACC vs. number of bins (H) for (a) SNR = 1.7 dB and (b) SNR = 8.6 dB.

Fig. 8(a) and 8(b) show the recognition accuracy versus number of bins (H) with different algorithms using 4-QAM, where $T = 1$ and SNR = 1.7 dB and 8.6 dB, respectively. As can be seen from the figures, the accuracy of the four classification algorithms increases with the increase of H under two SNR conditions, but it starts to decrease slightly after H

reaches 6. This is because as H increases, the feature representation becomes finer, which helps the classification algorithms to capture more details of the signal, thus improving the accuracy. However, high H may lead to overfitting and noise introduction, resulting in lower accuracy. Specifically, at 8.6 dB, when H is increased from 2 to 4, the accuracy of k-NN improves by 26%. When H = 6, the classification algorithm has reached a stable performance, at which point continuing to increase the number of bins has limited improvement in accuracy.

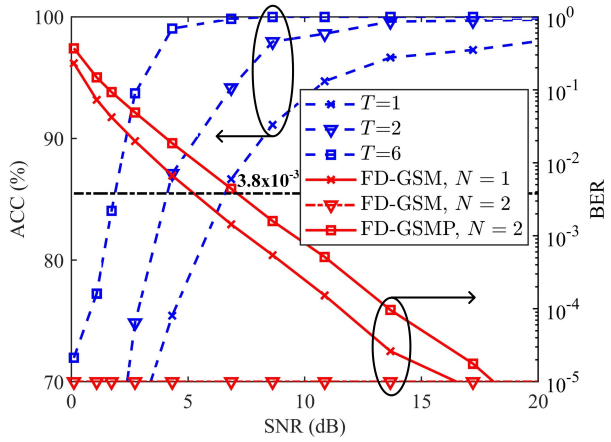

Fig. 9. Simulation accuracy and BER vs. SNR over an AWGN channel.

Fig. 9 shows the simulation accuracy and BER vs. SNR over an additive white Gaussian noise (AWGN) channel using 4-QAM with H = 10 and k-NN. With the increase of SNR, the BER gradually reduces while the accuracy gradually increases. Specifically, FD-GSM with $N = 1$ requires 5.2 dB to reach the 7% forward error correction (FEC) coding threshold (BER $= 3.8 \times 10^{-3}$), whereas FD-GSMP with $N = 2$ requires 6.8 dB to achieve the same threshold. For FD-GSM with $N = 2$, the BER remains consistently zero due to identical signal transmission and difference processing at the receiver. Moreover, when $T = 6$ at approximately 5.2 dB, the accuracy exceeds 99%. These results demonstrate that increasing the number of OFDM symbols can effectively enhance recognition performance, particularly in low SNR conditions.

V. Conclusion

In this paper, we firstly propose an intelligent modulation recognition scheme for two frequency-domain based transmission schemes and the number of activated LEDs in indoor GO-MIMO systems, which has the advantages of low complexity and easy implementation. The frequency-domain difference amplitude histogram is used as the recognition feature, and various machine learning or deep learning algorithms are used to achieve efficient intelligent modulation recognition for small sample data. Simulation results show that compared with other recognition algorithms, k-NN achieves better recognition performance at low SNRs. Meanwhile, by increasing the number of symbols to generate the feature histograms, high–accuracy recognition at low SNRs can be achieved.

References

[1] Narendra Vishwakarma and Swaminathan R, "On the Capacity Performance of Hybrid FSO/RF System With Adaptive Combining Over Generalized Distributions," IEEE Photonics Journal, vol. 14, no. 1, pp. 1–12, Feb. 2022.

[2] J. M. Chen, B. H. Deng, C. Chen, M. Liu, H. Y. Fu, and H. Haas, "Efficient capacity enhancement using OFDM with interleaved subcarrier number modulation in bandlimited UOWC systems," Optics Express, vol. 31, no. 19, pp. 30723–30723, Aug. 2023.

[3] J. An, C. Xu, Y. Liu, L. Gan, and L. Hanzo, "The Achievable Rate Analysis of Generalized Quadrature Spatial Modulation and a Pair of Low-Complexity Detectors," IEEE Transactions on Vehicular Technology, vol. 71, no. 5, pp. 5203–5215, May 2022.

[4] S. P. Alaka, T. Lakshmi Narasimhan, and A. Chockalingam, "Generalized Spatial Modulation in Indoor Wireless Visible Light Communication," 2015 IEEE Global Communications Conference (GLOBECOM), Dec. 2015.

[5] C. Chen, X. Zhong, S. Fu, X. Jian, M. Liu, H. L. Yang, A. Alphones, and H. Y. Fu, "OFDM-Based Generalized Optical MIMO," Journal of Lightwave Technology, vol. 39, no. 19, pp. 6063–6075, Jul. 2021.

[6] Q. W. He, Z. H. Zeng, M. Liu, B. B. Zhu, B. Lin and C. Chen, "AI-enabled efficient modulation classification in underwater OWC systems," Optical Review, Oct. 2024.

[7] X. Y. Zhang, Z. H. Zeng, P. F. Du, B. J. Lin, and C. Chen, "Intelligent index recognition for OFDM with index modulation in underwater OWC systems," IEEE Photonics Technology Letters, vol. 36, no. 20, pp. 1249–1252, Oct. 2024.

[8] Y. N. Zhao, C. Chen, Z. H. Zeng, Y. H. Yin, H. L. Cao, H. Haas, "Intelligent automatic modulation recognition for OFDM with index modulation in underwater OWC systems," Optics Letters, vol. 50, no. 10, pp. 3177–3180, May 2025.

[9] Merih Leblebici, A. Çalhan, and Murtaza Cicioğlu, "CNN-based automatic modulation recognition for index modulation systems," Expert Systems with Applications, vol. 240, pp. 122665–122665, Nov. 2023.

[10] Y. N. Zhao, C. Chen, H. L. Cao, Z. H. Zeng, M. Liu, and H. Haas, "Intelligent open-set MIMO recognition in OWC using a Siamese neural network," Optics Letters, vol. 49, no. 24, p. 7060, Dec. 2024.

[11] T. Komine and M. Nakagawa, "Fundamental analysis for visible-light communication system using LED lights," IEEE Transactions on Consumer Electronics, vol. 50, no. 1, pp. 100–107, Feb. 2004.

[12] Y. X. Cui, C. Chen, Y. P. Cai, Z. H. Zeng, M. Liu, J. Ye, S. H. Shao, and H. Haas, "Retroreflective optical ISAC using OFDM: Channel modeling and performance analysis," Optics Letters, vol. 49, no. 15, pp. 4214–4217, Aug. 2024.